Stress Intensity Factor For Aluminum And Copper Spot Weld Joints

Marwah Sabah Fakhri[1,2], Ahmed Al-Mukhtar[3,4*], and Ibtihal A. Mahmood[2]

[1] Ministry of Higher Education and Scientific Research-Baghdad, Iraq
[2] University of Technology-Iraq, Mechanical Engineering Department, Baghdad, Iraq
[3] College of Engineering, Al-Hussain University College, Iraq
[4] Institute of Structural Mechanics, Bauhaus-Universität Weimar, Germany
[*] Corresponding author. E-mail: almukhtar@structuralintegrity.eu

Received: January 27, 2024; Accepted: July 22, 2024

For decades, resistance spot welding (RSW) between aluminum and copper has encountered difficulties; however, it remains essential for modern applications. Additionally, crack propagation and the stress intensity factor (SIF) of dissimilar RSW have not been extensively investigated. The welding parameters used for Al-Al joints were as follows: welding current, time, and electrode force were set at 14,000 Amps, 0.8 seconds, and 7,000 N, respectively. Conversely, for Al-Cu joints, 14,000 Amps, 1 second, and 8,800 N were determined. The similar joints exhibited an average weld nugget size of 6 mm, whereas the dissimilar joints had a nugget size of 5.2 mm. The tensile shear force was 690 N and 780 N for dissimilar and similar joints, respectively. Accordingly, the fatigue load, as a percentage of the tensile force, was utilized at 414 N and 468 N for Al-Cu and Al-Al, respectively. Finite Element Analysis (FEA) was employed to determine the SIF. The initial crack length was determined to be 0.1 mm. The numerical solution was then compared with theoretical solutions for the opening SIF-KI, such as the equations proposed by Pook and Zhang. The FEA results showed higher values of SIF compared to those from theoretical solutions. Additionally, crack propagation was investigated for both dissimilar and similar joints at a determined failure load. Cracks tended to develop close to the heat-affected zone (HAZ) around the weld nugget diameter (d_n). SIF and crack path have been verified.

Keywords: Aluminum; Copper; Crack; Fracture; Resistance spot welding; Stress intensity factor

http://dx.doi.org/10.6180/jase.202507_28(7).0003

1. Introduction

RSW is a solid-state joining method that involves heating the connecting surfaces of sheet metal components. In mechanical engineering, especially in the automotive sector, copper and aluminum are commonly utilized in sheet form [1]. These metals possess a variety of qualities, including excellent fatigue resistance, strong electrical conductivity, and resistance to corrosion. Due to its effectiveness and dependability, RSW is the most popular sheet joining technique for structures and assembling the automotive parts [2]. For cyclically loaded structures, fatigue becomes a serious issue, such as in car chassis and aviation construction [3–5]. Since, the weld joints area suffering from cracks, the fatigue toughness in terms of SIF have to be considered [6–8]. Understanding the fatigue behavior of resistance spot welding (RSW) is crucial to ensuring the reliability and safety of welded structures, as fatigue can lead to the initiation and propagation of fractures [9–12]. In this context, the SIF stands out as one of the most critical and practical parameters in the field of fracture mechanics. It describes the stress condition at the crack tip and controls the crack propagation in structures [13, 14]. The SIF plays a pivotal role in determining whether a crack will propagate in a given material under specific loading conditions [15]. The calculation of SIF involves evaluating stress distribution around the crack tip and considering factors such as geom-

etry, loading mode, and crack size [16, 17]. Considering the opening-SIF at the crack tip as a driving force for crack propagation is called the linear elastic fracture mechanics approach (LEFM), which assumes the existence of an identified crack [18–20]. LEFM assumes only one crack for propagation and SIF calculation. Additionally, since LEFM considers opening-SIF, residual stresses and closure effects are very simple [14, 21].

Numerous research studies have been conducted to study the fatigue behavior and SIFs of cracks in welded joints based on LEFM [12, 22, 23]]. They found that this approach can be used for spot welding in through thickness crack in spot weld using FEM. Banerjee et al [12] found that the fatigue properties are related to the weld nugget size and consequently to the heat input parameters. Pan et al [24] used FEM and compared the results with literature. They found an agreement with Zhang's equation [25].

Several studies have involved experimental testing, numerical simulations using FEA, and principles of fracture mechanics for dissimilar metals with steel alloys. Kim et al [26] investigated the spot joining of aluminum and steel to achieve lightweight vehicles. They determined the optimum welding parameters.

Spot joining of aluminum and copper dissimilarly is challenging. Therefore, aluminum and copper are usually welded using friction stir spot welding [27]. In addition, the fracture mechanics of such joints, including SIF calculations, do not exist.

This research aims to numerically determine the SIF solution and validate the results by comparing them with available solutions from the literature, such as the equations proposed by Pook [28], and Zhang [25]. The FE model was developed using ABAQUS based on LEFM. Additionally, SIF and crack length (a) were calculated for both similar and dissimilar joints. The current model was validated by comparing the SIF solution and the crack path for Al-Al and Al-Cu RSW.

2. Methodology

This work encompasses experiments, numerical, and analytical calculations. The following chart gives insight into the methodology used in this work, see Fig. 1. The validations have been achieved by comparing the experimental, analytical, and simulation results for the crack path and SIF calculations.

2.1. Materials

Copper and aluminum sheet alloy, 1 mm thickness was used. The proposed applications and the aims of such metals are electrical conductivity, and fracture toughness for electric cars and similar aspects. The chemical composition, tensile test, and microstructure test, were conducted to determine the based metal properties.

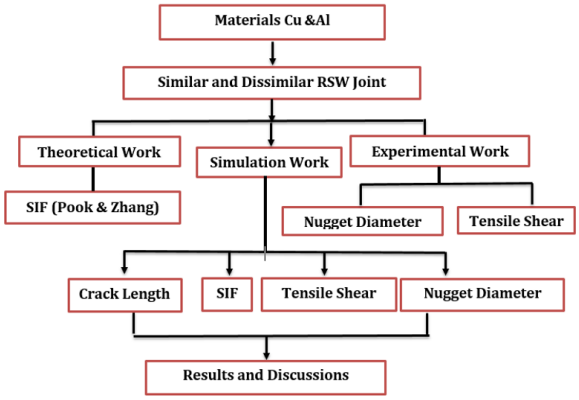

Fig. 1. Schematic flow chart of the methodology.

The selected materials for this study consist of commercially pure copper sheet of T2 grade and aluminum AA1050 (part of the AA 1XXX series). The chemical composition analysis for Al-1050, and pure copper T2 grade was carried out; see Tables 1 and 2, respectively.

2.2. Tensile Test

The sheet specimens for the as-received metals are prepared using a CNC machine in accordance with the standard specifications ASTM E8/E8M13a [29]; see Fig. 2. Samples are cut with the rolling directions to calculate the ultimate tensile stress. The rolling sheet direction has a larger ultimate [30]. Hence, the specimens were cut in the direction of rolling, which exhibited a slightly higher tensile force owing to the elongated grain structure.

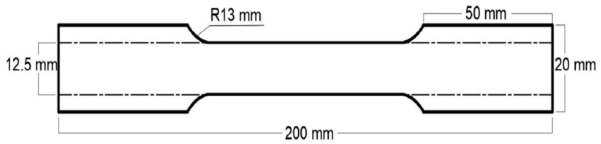

Fig. 2. Tensile specimen and dimensions.

Three samples were taken for each case; hence the average values have been used, see Fig. 3. The tensile test was carried out using a universal testing machine with a speed rate of 1 mm/min.

The tensile force, yield strength, elongation, and Young's modulus, have been presented in Table 3. These values will be used as an input data for FE model in ABAQUS. In addition, the physical properties (Table 4).

Table 1. Chemical compositions of Al-1050.

	Element %							
Material	**Si**	**Fe**	**Cu**	**Mn**	**Mg**	**Zn**	**Ti**	**AL**
Al-1050	0.047	0.4	0.048	0.0033	0.0012	0.0027	0.021	99.5

Table 2. Chemical compositions of pure copper T_2 grade.

	Element %									
Material	**Zn**	**Pb**	**P**	**Mn**	**Fe**	**Ni**	**Si**	**Mg**	**AL**	**Cu**
Cu	0.003	0.0003	0.0008	0.0004	0.007	0.0002	0.0008	0.0001	0.002	≈ 100

Fig. 3. Specimens configuration and the fracture mode.

Table 3. Mechanical properties of Al-1050 and Cu.

	Mechanical Properties			
Metals	$\sigma_{y(}$**(MPa)**	σ_{yts}**(MPa)**	E (GPa)	El. %
Cu	144	209	129	34
Al	80	112	67	7.8

2.3. RSW Joints

2.3.1. RSW Processing

Due to the resistance to the current flow, the localized heat between the two surfaces will produce a weld of molten metal. The weld nugget occurs at the interface between two surfaces as the metal surfaces start to melt [33]. Two opposite electrodes are used to fix the two sheets of metal during the weld and to solidify the weld area afterward, see Fig. 4. The RSW process and specimen dimensions have been determined according to the EN ISO 14329 standard [34, 35]. The welding machine used is a rocker-arm foot-operated pneumatic spot-welding machine labeled as SIP column-PPV50.

2.3.2. Welding Parameters

Welding parameters are chosen either by conducting tensile tests or by using analytical data analysis. The Taguchi approach was used in this study as the design of the engineering tool. It's an engineering method of product or process design that focuses on minimizing variance and/or sensitivity. It was applied using a Minitab program, which determined the values of the expected welding parameters. Therefore, the output parameters of Taguchi were used as variables in the experimental work to obtain the optimal weld joint. Welding parameters are among the most essential work steps, especially in dissimilar RSW [36, 37].

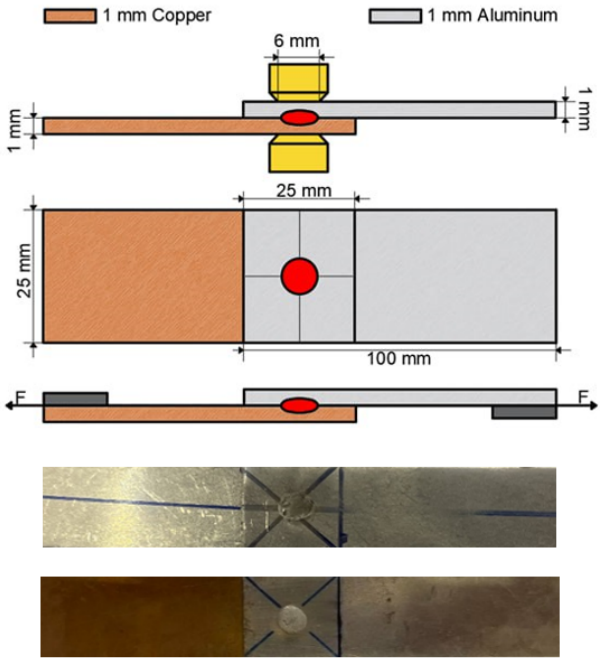

Fig. 4. Specimen configurations and dimensions.

Three values for each welding parameter were used in the Taguchi approach (input data), as shown in Table 5. The input parameters were used for lap-shear specimens made from either similar or dissimilar sheet combinations. For welding similar materials, the welding parameters were specified in accordance with the AWS C1.1 M/C1 standard [38, 39]. Table 5 shows the optimum RSW parameters that was used.

Then, these values have been optimized by the Taguchi method to reduce the number of tested specimens and obtain high-quality and robust welding, see Table 6.

For Al-Cu joints, the optimum input welding parameters were determined according to the sheet thicknesses after a few trials and tests. Then, conduct a traditional tensile test to determine the maximum tensile force. Then, the experiment's results have been verified using the Taguchi approach [40]. It was found that the energy produced dur-

Table 4. Physical properties of Al-1050 and Cu [31, 32].

Properties	Unit	Al	Cu
Density	g/cm^3	2.70	8.94
Resistance	$(\Omega mm^2/m) \times 10^2$	2.66	1.68
Thermal Conductivity	$cal^\circ cm^2/cm^\circ Cs$	0.52	0.92
Thermal Coefficient of Linear Expansion	$(mm/mm^\circ C) \times 10^{-6}$	24.00	16.70
Specific Heat Capacity	$J/kg^\circ C$	902	385
Melting Temperature	$^\circ C$	660	1083
Poisson Ratio	–	0.31	0.33

Table 5. RSW Parameters Used in Taguchi (input data).

Welding Current (Amp.)	Electrode Force (N)	Welding Time (Sec)
10000	6280	0.8
12000	7540	0.9
14000	8800	1

Table 6. RSW parameters for Al-Al joints.

Joint type	Current (Amp.)	Electrode Force (N)	Weld time (sec)
Al-Al [38]	14000	7000	0.8

ing welding depends on the electrical current, the time of the current flows, and resistance that may also be altered [41]. The major effects graphic shows that the response variable (i.e., tensile force) seems to be influenced by all of the parameters; see Fig. 5. Therefore, the optimum RSW parameters have been chosen at maximum tensile shear force; see Table 7.

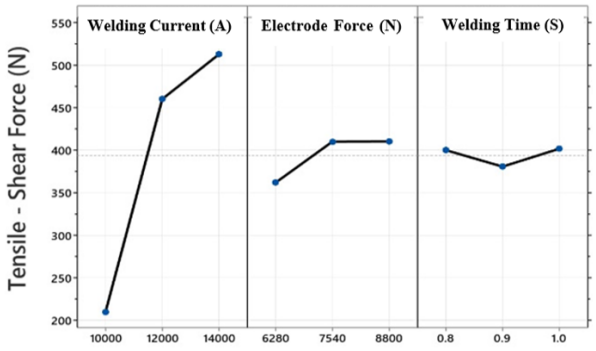

Fig. 5. RSW parameters effect on the TS, Taguchi technique.

2.3.3. *Nugget Diameters Measurement*

The diameter of the nugget (d_n) is one of the most critical parameters. It was calculated for Al-Al, and Al-Cu after welding. Three sample each set of parameters were taken to determine dn. In case of dissimilar joints (Al-Cu), dn from two sides were calculated. Because, the weld nugget diameters are different at each side. The metals differ in the amount of developed heat; hence, the weld area will be developed accordingly. The machine electrode diameter is 6 mm. The nugget diameter calculated by using a Vernier; see Fig. 6.

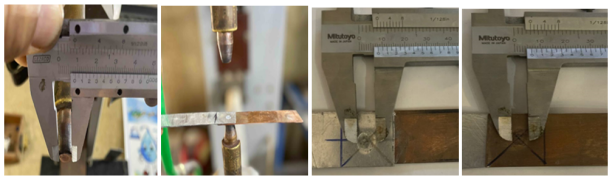

Fig. 6. Electrode face diameter in RSW machine and nugget diameters measurements.

2.3.4. *Tensile Shear Test*

The tensile test spot weld specimens were prepared according to the EN ISO 14329 standard [39]. Two sheets, 100 mm long and 25 mm wide, with a thickness of 1 mm and overlapping 25 mm, have been welded (Fig. 4). A shim plate is recommended be used in the gripping jaws [42], to ensure that the axial load is applied to the single spot weld (Fig. 7a). A universal testing equipment with a 1 mm/min deformation rate was used (Fig. 7b). To improve the accuracy of the tensile shear test findings, the experiments were repeated, and

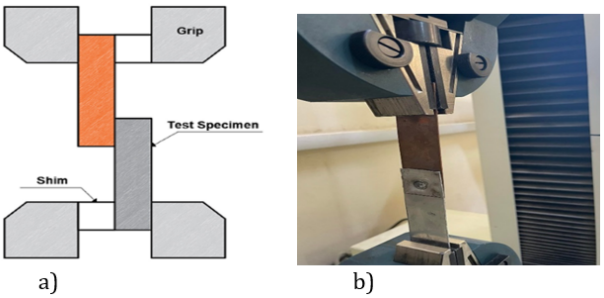

Fig. 7. Tensile Shear Test; a) Shims, b) Universal testing machine, Tinius Olsen H50 KT.

Table 7. RSW parameters for Al-Cu joints.

Joint	Welding current (Amp.)	Electrode force (N)	Welding time (sec)
Al-Cu	14000	8800	1

2.3.5. Finite Element Models

ABAQUS-FE software simulator was used to determine the crack propagation and SIF in similar and dissimilar RS joints based on the LEFM. The preprocessing steps included creating a 3D model of the RSW joint, subdividing the geometry, and generating meshes. The current model typically involves creating a circular region representing the nugget zone and considering the heat generation, developing the nugget accordingly, and crack initiation and propagation consequently; see Fig. 8.

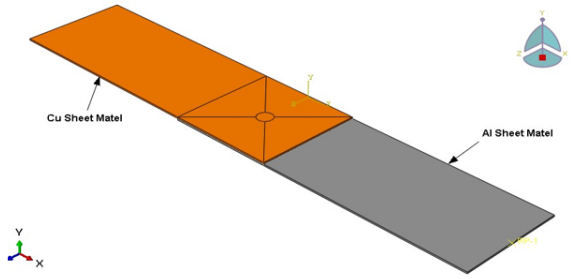

Fig. 8. RSW FE-model.

LEFM principles are employed to assess crack propagation and SIF calculations by performing advanced ABAQUS features. This model can be used to provide a comprehensive understanding of fracture mechanics under cyclic loading conditions [18, 19]. Von Mises stress is an important factor in RSW. It can be used to predict the stress concentration and load-bearing capacity of welded joints. The maximum stress is found around the weld nugget areas [43]. Nevertheless, the crack location was also validated by the tensile and fatigue tests. The initial crack is located at the maximum stresses, a_i= 0.1 mm; see Fig. 9.

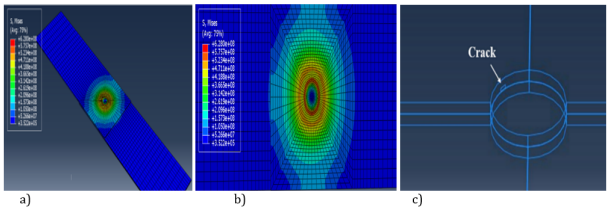

Fig. 9. a) and b) Von Mises stresses and initial crack in weld nugget; c) Initial crack occurs at the maximum stress sites for crack length to width ratio a/c=1.

In ABAQUS, the meshing process involves discretizing a 3D model into FE. Defining the element size for the mesh is very important. The work piece was meshed with 3D linear hexahedral elements of type C3D8R; see Fig. 10a [44]. These elements are commonly employed in FEA for their suitability in capturing complex geometric shapes and structural behavior. Overall, the use of hexahedral meshing in welding simulation typically results in more accurate, stable, and computationally efficient outcomes compared to other meshing techniques. The mesh size is distributed gradually along the specimens; see Fig. 10b.

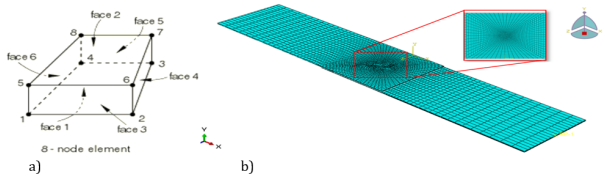

Fig. 10. a) 3D Element 8-node type C3D8R; b) Mesh generation for RSW.

The accurate number of elements to mesh the plate selecting by mesh convergence test. In order to prevent the outcomes of an analysis from being impacted by changing the size of the mesh, mesh convergence refers to the smallness of the elements needed in a model [45, 46]. The convergence analysis is carried out to ascertain the precise number of elements to mesh the sheet and get the right outcome with the least amount of program execution time. The effect of meshes and elements on the stress was examined; see Fig. 11. Therefore, the mesh consists of a total of 25,784 nodes and 21,160 elements (Table 8). The welding zone features a finer mesh region, indicating that the meshing is appropriate for this situation.

Table 8. Mesh convergence effect.

Nr. Elements	Max. Mises Stress (MPa)
8777	8.5×107
10520	1.1×108
15780	5.42×108
21160	6.1×108
50495	6.21×108

In order to conduct an accurate simulation, input conditions such as material properties (e.g., elastic modulus, yield strength, and Poisson's ratio) were defined (Tables 3 and 4). Additionally, the optimum RSW parameters

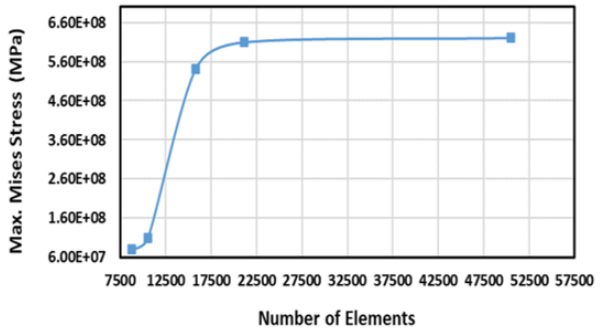

Fig. 11. Meshes effect on the stresses of RSW joints.

for both similar and dissimilar joints were selected; refer to Tables 5 and 6. Moreover, to conduct the SIF analysis and crack propagation, the critical fracture toughness (KIC) is taken as an average values 25 MPa.m$^{0.5}$ and 30 MPa.m$^{0.5}$, and the threshold Kth is taken as 4 MPa.m$^{0.5}$ and 5 MPa.m$^{0.5}$ for copper and aluminum, respectively [47].

Additionally, appropriate boundary conditions should be applied to replicate the actual loading conditions experienced by the welded joint. One side end will be fixed, and the other side will be exposed to cyclic loading. Then, apply the loading conditions to simulate the tensile shear test. This typically involves defining a force boundary condition on one side of the joint while fixing the opposite side; see Fig. 12 (a and b). The postprocessing will show the results, including stress, SIF, crack propagation, and deformation.

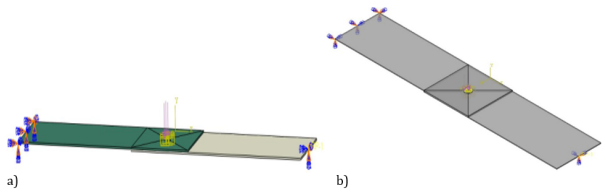

Fig. 12. a) and b) Boundary condition of dissimilar and similar RSW joints, respectively.

2.3.6. *Stress Intensity Factors*

SIFs are inevitable parameters in fracture mechanics methods. The SIF is particularly relevant when considering defects, cracks, or notches near the weld nugget. It helps predict whether these defects can propagate and lead to joint failure under applied loads, hence, ensuring the safety and integrity of the weld joints [8, 48]. Therefore, these factors describe the fatigue behavior at a crack tip in terms of crack propagation [49]. Initial cracks (a_i) are initiated and propagate to a final length (a_f) under cyclic loading [50].

The opening Mode-I is more common under axial tensile fatigue test conditions. Fatigue loading involves cyclic forces, such as tension-compression cycles, that are applied to the welded joint. Over time, these cyclic stresses can lead to crack initiation and propagation [16].

SIF can be determined using various mathematical equations Pook, Zhang, Swelem and FE-numerical methods. The Pook and Zhang method is based on the assumption that the nugget has a circular shape while the Swelem method is based on the assumption that the nugget has an elliptical shape [25, 51]. The SIF of the initial cracks around the nugget were calculated according to Pook's Eq. (1) and Zhang Eq. (2), respectively [24].

$$KI = \frac{F}{(d/2)^{3/2}}\left[0.341\left(\frac{d}{t}\right)^{0.397}\right] \quad (1)$$

$$KI = \frac{\sqrt{3}F}{2\pi d\sqrt{t}} \quad (2)$$

where KI is SIFs under opening Mode-I. F is the applied loads per spot weld, d is the nugget diameter, and t is the sheet thickness.

To calculate SIF and determine the crack propagation numerically, the fatigue test option in ABAQUS was used. In addition, a minimum to maximum stress ratio of R= 0.1 was used. The fatigue test load is started at 60% of the maximum tensile shear load [52].

2.3.7. *Crack Propagation*

Crack propagation occurs when the stress at the crack tip reaches the threshold fracture toughness (Kth). Fatigue loads and vibrations under cyclic loading will propagate the crack, leading to fatigue failure [53]. Cyclic loading, in the form of vibrations, can cause failure even under relatively light loads [35, 54]. The existing crack in the weld nugget will start to grow, and the crack length will increase as the SIF increases. The fatigue crack propagation of RSW for Al-Al and Al-Cu joints is investigated based on the LEFM approach using FEM.

3. Result and discussion

3.1. Nugget Diameters Measurement

FE thermal simulation will develop the proposed weld area according to heat input and material input properties. Hence, the nugget diameter was estimated from the FE simulation in addition to the experiment measurement. Table 9 shows the nugget diameter for similar and dissimilar RSW, which is determined experimentally and numerically using ABAQUS. It was shown that there are differences in nugget diameter in the case of Al-Cu welding. The nugget

on the Cu-side is smaller than on the Al-side, likely due to higher heating levels on the Al-side compared to the Cu-side. In the case of Al-Al welding, the weld nugget diameter is approximately equal. Changes in the nugget size can influence the SIF [55].

Table 9. Nugget diameter for dissimilar RSW Joint.

	d_n (mm) $\pm$ 0.1 mm	
RSW Joints	Experimental	Simulation
Al − Cu, Al side	5.8	5.721
Al − Cu, Cu side	4.6	4.61
Al − Al	6	5.99

The differences in nugget diameter on the two sides of dissimilar metals due to the effect of the material's thermal properties. Hence, the average nugget diameters will be used in Eqs. (1) and (2) to calculate SIF.

3.2. Tensile Shear Force

The force of the overlapping RSW joints was assessed using tensile shear tests. Table 10 shows the experimental and numerical results for Al-Al, and Cu-Al joints. The values have been compared with the literature. Hence, the current model and condition has been verified.

Table 10. Tensile force, TF of RSW joints.

Joints	TF (N), Experiment	TF (N), FE	TF, literature (N)
Cu-Al	690	842	680 [56]
Al-Al	780	912	750 [57]

The tensile shear force for dissimilar RSW is lower than those of similar RSW due to the differences in material properties that can lead to variations in weld quality [58].

3.3. Stress Intensity Factor Calculation

SIF has been calculated using analytical and FE methods. Hence, the relation between SIF and applied force has been presented. In addition, numerical simulation shows the relationship of a-SIF.

3.3.1. SIF for Similar and Dissimilar RSW

As described earlier, the SIF was calculated at fatigue loads starting from 60% of the experienced tensile load of the weld nugget [52]. Traditionally, increasing the weld nugget size causes an increase in tensile force or failure load. Therefore, as the weld nugget and failure load increase, the SIF also increases, as seen in Fig. 13.

Pook and Zhang (Eqs. (1) and (2)) developed a straightforward equation for RSW joints under tensile shear to determine SIF [24]. These equations were used to calculate the SIFs at average nugget diameters of 6 mm and 5.2 mm for similar and dissimilar joints, respectively. The results were then compared with the FE solution of the SIF.

Once again, the loads applied to the FE model depended on the tensile-shear test [52]. Tables 11 and 12 show the results for SIF for dissimilar and similar RSW numerically and analytically.

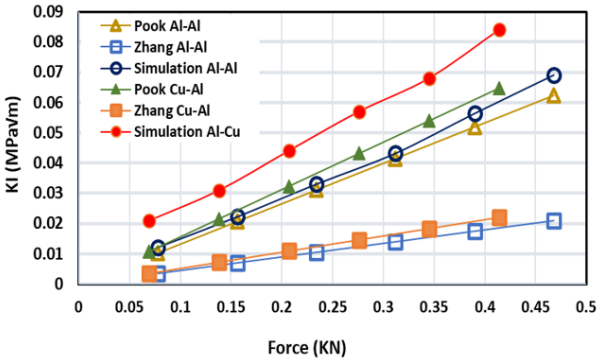

Fig. 13. Relationship of SIF and Load at fatigue load starting at F = 10%, 20%, 30%, 40%, 50%, and 60% of TS = 780 N and 690 N; d_n = 6 mm and 5.2 mm for Al-Al and Al-Cu, respectively

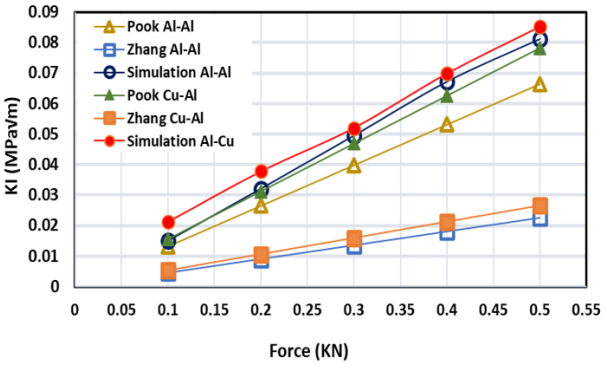

Fig. 14. Relationship between SIF and Load at d_n = 6 mm and 5.2 mm for Al-Al and Al-Cu, respectively.

There are a differences in fatigue failure and cracking when dissimilar materials are joined by using RSW, the differences in their mechanical properties, such as stiffness or thermal expansion coefficients, can create stress concentrations at the interface [22].

In contrast, similar welded joints produce higher material homogeneity resulting in a more uniform stress distribution across the weld joint. This minimizes stress concentrations and decreases SIF at the crack tip. Additionally, similar materials typically have compatible coefficients of thermal expansion, reducing the risk of differential expan-

Table 11. SIF value for Al-Cu RSW joint, d_n=5.2 mm, Max. Force=690 N

ST (kN)	D (mm)	Max. Applied Load (kN)	KI Max. (MPa$\sqrt{m}$) Pook	KI Max. (MPa$\sqrt{m}$) Zhang	KI Max. (MPa$\sqrt{m}$)
0.69	5.2	0.069	0.0107	0.0036	0.021
0.69	5.2	0.138	0.0215	0.0073	0.031
0.69	5.2	0.207	0.0323	0.0109	0.0441
0.69	5.2	0.276	0.0431	0.0146	0.057
0.69	5.2	0.345	0.0539	0.0182	0.068
0.69	5.2	0.414	0.0647	0.0219	0.084

Table 12. SIF value for Al-Al RSW joint, d_n=6 mm, Max. Load=780 N

ST (kN)	D (mm)	Max. Applied Load (kN)	KI Max. (MPa $\sqrt{m}$) Pook	KI Max. (MPa $\sqrt{m}$) Zhang	KI Max. (MPa $\sqrt{m}$)
0.78	6	0.078	0.0103	0.00351	0.0121
0.78	6	0.156	0.0207	0.00702	0.0222
0.78	6	0.234	0.0311	0.01053	0.033
0.78	6	0.312	0.0414	0.01404	0.0432
0.78	6	0.39	0.0518	0.01755	0.0564
0.78	6	0.468	0.062	0.02106	0.0691

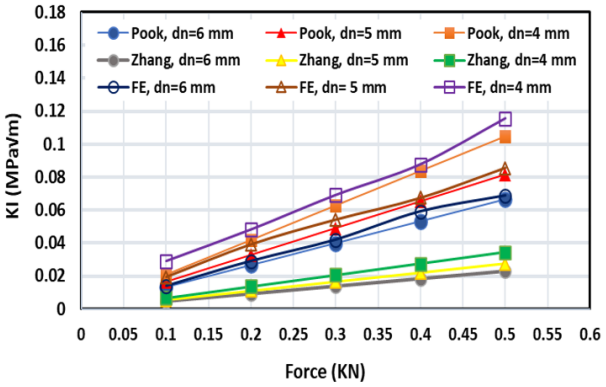

Fig. 15. Relationship between SIF and load, at different d_n using Pook, Zhang, and FE (ABAQUS).

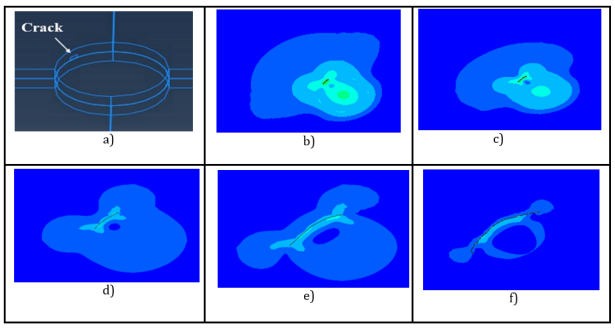

Fig. 16. FE simulation of crack growth; F=414 N, a_i=0.1 mm.

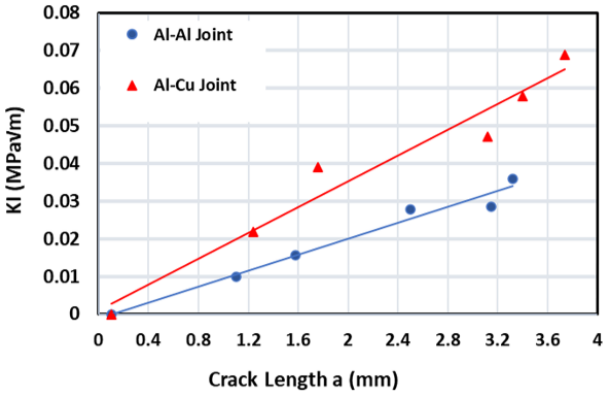

Fig. 17. SIF and crack length of RSW, ABAQUS.

sion and contraction during welding. Hence, reducing the effect of residual stresses [52]. The FE model shows higher values of SIF compared with the analytical solution of SIF from Zhang and Pook (see Figs. 13 and 14). This is because those analytical solutions do not consider factors such as metal type, crack length to width ratio, and thermal properties, which were taken into account in the numerical model.

To make a clear comparison, the same loading was used for both the analytical and FE models (Fig. 14). The same behavior was obtained.

The comparison between the FE model and the analytical solution of SIF is shown in terms of weld nugget area, see Fig. 15. The increase in SIF of the weld nugget area will decrease the SIF at the crack tip.

3.3.2. Relation of Crack Growth and SIF

The theoretical equation of SIF for RSW shows the relationship between SIF and metal thickness (t) rather than crack length (a). Therefore, the current model proposes such a

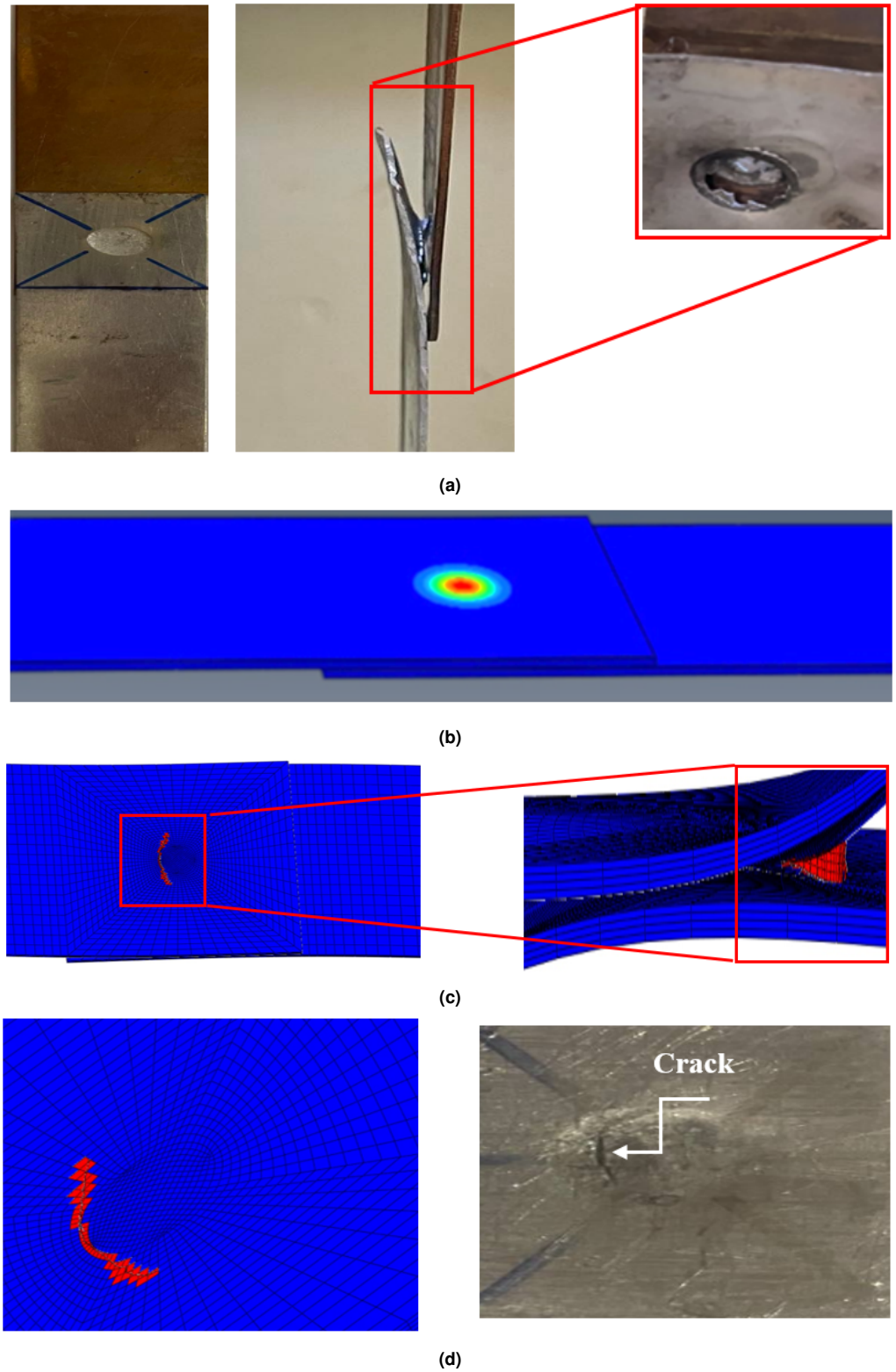

Fig. 18. Crack Propagation at R=0.1: a) during fatigue test; b), and c) FE simulation; d) Comparison between FE and experiments.

Table 13. SIF and crack length for RSW Joint by simulation.

Al-Cu Joint				Al-Al Joint			
TS (N)	F_{Max} (60% ST) (N)	KI (MPa $\sqrt{m}$)	a (mm)	TS (N)		KI (MPa $\sqrt{m}$)	a (mm)
690	0	0	0.1	780	0	0	0.1
690	414	0.0218	1.24	780	468	0.0099	1.1
690	414	0.0391	1.76	780	468	0.0157	1.58
690	414	0.0471	3.12	780	468	0.0278	2.93
690	414	0.0579	3.4	780	468	0.0286	3.145
690	414	0.0688	3.74	780	468	0.0359	3.321

relationship between SIF and a. Such a relationship is essential in fracture mechanics because. It helps in assessing the criticality of a crack or defect in a material or structure. A higher SIF indicates a greater crack propagation rate. A crack length of 0.1 mm was inserted in the FE model for sheet thickness 1 mm (see Fig. 16).

The crack was located at higher stress concentration area. The FE model shows the crack propagation and its path around the weld nugget; see Fig. 16, a-f. Table 13 shows the FE results value in terms of tensile shear force of metals (TS), applied fatigue load (F), and crack length (a). Fig. 17 shows the schematic FE-results of SIF versus crack length. As is known, increasing the crack length increases the SIF at the crack tip. Additionally, the values of SIF at the crack tip in dissimilar metals are higher than those in similar RSW metals.

As the crack length increases, the SIF also increases. Hence, a longer crack creates a larger stress concentration at its tip, decreasing the expected fatigue life.

3.4. Final Failure and Its Simulation

The pre-existing crack, caused by the notch around the weld nugget and between the two sheets, propagates through the sheet thickness and around the weld area due to the high stress concentration. The region around the weld nugget suffers from microcracks and residual stresses. Therefore, the spot weld failed in the form of a pullout failure mode under the fatigue load for dissimilar RSW joints (see Fig. 18).

4. Conclusion

This study investigates RSW joints for similar and dissimilar joints with thicknesses of 1 mm. The experiment and numerical simulation have been carried out. Hence, the experiments results have been compared and validated with numerical results. The following conclusions have been drawn from this study:

1. Welding parameters for both similar and dissimilar RSW metals have been verified and presented, including welding current, time, and electrode pressure.

2. Taguchi analysis data has been utilized to determine the optimum welding parameters.

3. Tensile shear tests have been conducted and compared with FE results to validate the FE model.

4. Additionally, an FE model has been developed to simulate crack initiation, propagation, and calculate SIF.

5. Linear Elastic Fracture Mechanics (LEFM) demonstrates validated results, confirming the accuracy of the current model.

6. Numerical SIF calculations have been compared with analytical solutions, showing good agreement.

7. It has been observed that cracks tend to grow around the spot-welding nugget and propagate under tensile and fatigue loading.

8. Increasing crack length results in higher SIF, thus reducing the structural integrity of the joints.

9. Al-Cu joints exhibit higher SIF at the crack tip compared to similar Al-Al joints. Additionally, increasing the weld area decreases SIF at the crack tip, improving fatigue life.

10. Dissimilar spot weld joints show lower tensile and fatigue toughness compared to similar joints, suggesting a need for modifications to enhance their strength in future work.

11. Future work may concern the modification of fracture toughness in RSW of dissimilar joints presented in this study, as such joints still suffer from lower toughness and crack initiation.

nomenclature

Acronyms

a	Crack length [mm]
a_f	Final crack length [mm]
a_i	Initial kinked Crack Length [mm]
a_i/d_n	Crack growth rate [mm/cycle]
Al-Al	Aluminium–Aluminium joint
Al-Cu	Aluminium–Copper joint
BM	Base metal
Cu-Cu	Copper–Copper joint
d_n	Spot weld or Nugget Diameter [mm]
E	Modulus of elasticity [N/mm^2]
FEA	Finite Elements Analyses
FZ	Fusion Zone
HAZ	Heat Affected Zone
KI	SIF- opening mode [MPa.mm$^{0.5}$]
KII	SIF-Sliding mode [MPa.mm$^{0.5}$]
RSW	Resistance Spot Welding
SIF (K)	Stress Intensity Factor [MPa.mm$^{0.5}$]

References

[1] M. S. Fakhri, A. Al-Mukhtar, and I. A. Mahmood, (2022) *"Comparative Study of the Mechanical Properties of Spot Welded Joints"* **Materials Science Forum *1079***: 21–28. DOI: 10.4028/p-488xsr.

[2] A. Al-Mukhtar, (2016) *"Review of Resistance Spot Welding Sheets: Processes and Failure Mode"* **Advanced Engineering Forum *17***: 31–57. DOI: 10.4028/www.scientific.net/AEF.17.31.

[3] A. Al-Mukhtar, (2019) *"Case Studies of Aircraft Fuselage Cracking"* **Advanced Engineering Forum *33***: 11–18. DOI: 10.4028/www.scientific.net/AEF.33.11.

[4] A. Al-Mukhtar, (2020) *"Aircraft Fuselage Cracking and Simulation"* **Procedia Structural Integrity *28***: 124–131. DOI: 10.1016/j.prostr.2020.10.016.

[5] A. M. Al-Mukhtar and Q. Doos, (2013) *"The Spot Weldability of Carbon Steel Sheet"* **Advances in Materials Science and Engineering *2013***: 1–6. DOI: 10.1155/2013/146896.

[6] A. M. Al-Mukhtar, T. Rahman, and Q. M. Doos. "Spot Welding Joint's Fracture Behavior and Fundamental". In: *Fracture, Fatigue and Wear*. 2019, 18–27. DOI: 10.1007/978-981-13-0411-8_2.

[7] M. Fakhri, A. Al-Mukhtar, and I. Mahmood, (2024) *"Effect of Mechanical Deformation on the Electrical Conductivity of Resistance Spot Welding Joints"* **Journal of Applied Science and Engineering (Taiwan) *27***(9): 3095–3103. DOI: 10.6180/jase.202409_27(9).0007.

[8] A. Al-Mukhtar, H. Biermann, S. Henkel, and P. Hübner, (2010) *"Comparison of the Stress Intensity Factor of Load-Carrying Cruciform Welded Joints with Different Geometries"* **Journal of Materials Engineering and Performance *19***(6): 802–809. DOI: 10.1007/s11665-009-9552-1.

[9] T. K. Pal and K. Bhowmick, (2012) *"Resistance Spot Welding Characteristics and High Cycle Fatigue Behavior of DP 780 Steel Sheet"* **Journal of Materials Engineering and Performance *21***(2): 280–285. DOI: 10.1007/s11665-011-9850-2.

[10] J. Ordoñez, R. Ambriz, C. García, G. Plascencia, and D. Jaramillo, (2019) *"Overloading effect on the fatigue strength in resistance spot welding joints of a DP980 steel"* **International Journal of Fatigue *121***: 163–171. DOI: 10.1016/j.ijfatigue.2018.12.026.

[11] H. T. Kang, A. Khosrovaneh, H. Hu, and U. De Souza. "A Fatigue Prediction Method for Spot Welded Joints". In: 2013, 2013–01–1208. DOI: 10.4271/2013-01-1208.

[12] P. Banerjee, R. Sarkar, T. Pal, and M. Shome, (2016) *"Effect of nugget size and notch geometry on the high cycle fatigue performance of resistance spot welded DP590 steel sheets"* **Journal of Materials Processing Technology *238***: 226–243. DOI: 10.1016/j.jmatprotec.2016.07.023.

[13] A. M. Almukhtar. *Fracture simulation of welded joints*. Nova Science Publishers Hauppauge, NY, USA, 2011.

[14] A. M. Al-Mukhtar, (2013) *"Investigation of the Thickness Effect on the Fatigue Strength Calculation"* **Journal of Failure Analysis and Prevention *13***(1): 63–71. DOI: 10.1007/s11668-012-9629-2.

[15] S. Zhang, (1999) *"Approximate stress intensity factors and notch stresses for common spot-welded specimens"* **Welding Journal *78***:

[16] J. Zhang, P. Dong, and Y. Gao. "Evaluation of Stress Intensity Factor-Based Predictive Technique for Fatigue Life of Resistance Spot Welds". In: 2001, 2001–01–0830. DOI: 10.4271/2001-01-0830.

[17] D. Wang, S. Lin, and J. Pan, (2005) *"Stress intensity factors for spot welds and associated kinked cracks in cup specimens"* **International Journal of Fatigue *27***(5): 581–598. DOI: 10.1016/j.ijfatigue.2004.08.008.

[18] D.-A. Wang and J. Pan, (2005) *"A computational study of local stress intensity factor solutions for kinked cracks near spot welds in lap-shear specimens"* **International Journal of Solids and Structures *42***(24-25): 6277–6298. DOI: 10.1016/j.ijsolstr.2005.05.036.

[19] R. I. Stephens and H. O. Fuchs, eds. *Metal fatigue in engineering*. 2nd ed. New York: Wiley, 2001.

[20] U. Zerbst, M. Madia, and H. Beier, (2017) *"Fatigue strength and life determination of weldments based on fracture mechanics"* **Procedia Structural Integrity *7***: 407–414. DOI: 10.1016/j.prostr.2017.11.106.

[21] A. M. Al-Mukhtar, (2013) *"Consideration of the residual stress distributions in fatigue crack growth calculations for assessing welded steel joints"* **Fatigue & Fracture of Engineering Materials & Structures *36***(12): 1352–1361. DOI: 10.1111/ffe.12060.

[22] D.-A. Wang, P.-C. Lin, and J. Pan, (2005) *"Geometric functions of stress intensity factor solutions for spot welds in lap-shear specimens"* **International Journal of Solids and Structures *42***(24-25): 6299–6318. DOI: 10.1016/j.ijsolstr.2005.05.037.

[23] Y. Uematsu and K. Tokaji, (2009) *"Comparison of fatigue behaviour between resistance spot and friction stir spot welded aluminium alloy sheets"* **Science and Technology of Welding and Joining *14***(1): 62–71. DOI: 10.1179/136217108X338908.

[24] N. Pan and S. D. Sheppard, (2002) *"Stress intensity factors in spot welds"* **Engineering Fracture Mechanics *70***(5): 671–684. DOI: https://doi.org/10.1016/S0013-7944(02)00076-0.

[25] S. Zhang, (1997) *"Stress intensities at spot welds"* **International Journal of Fracture *88***(2): 167–185. DOI: 10.1023/A:1007461430066.

[26] Y.-G. Kim, B.-J. Jo, J.-S. Kim, and I.-J. Kim, (2017) *"A study on dissimilar welding of aluminum alloy and advanced high strength steel by spot welding process"* **International Journal of Precision Engineering and Manufacturing *18***(1): 121–126. DOI: 10.1007/s12541-017-0015-6.

[27] M. Li, C. Zhang, D. Wang, L. Zhou, D. Wellmann, and Y. Tian, (2019) *"Friction Stir Spot Welding of Aluminum and Copper: A Review"* **Materials *13***(1): 156. DOI: 10.3390/ma13010156.

[28] L. P. Pook, (1975) *"Fracture mechanics analysis of the fatigue behaviour of spot welds"* **International Journal of Fracture *11***(1): 173–176. DOI: 10.1007/BF00034726.

[29] ASTM E8. *ASTM E8/E8M standard test methods for tension testing of metallic materials 1*. 2010. DOI: 10.1520/E0008.

[30] T. Wang, T. Zhu, J. Sun, R. Wu, and M. Zhang, (2015) *"Influence of rolling directions on microstructure, mechanical properties and anisotropy of Mg-5Li-1Al-0.5Y alloy"* **Journal of Magnesium and Alloys *3***(4): 345–351. DOI: 10.1016/j.jma.2015.11.001.

[31] İ. Ay, S. Çelik, and İ. Çelik, (2000) *"Comparison of properities of friction and diffusion welded joints made between the aluminium and copper bars"* **Balıkesir Üniversitesi Fen Bilimleri Enstitüsü Dergisi *2***(1): 88–102.

[32] P. Kah, C. Vimalraj, J. Martikainen, and R. Suoranta, (2015) *"Factors influencing Al-Cu weld properties by intermetallic compound formation"* **International Journal of Mechanical and Materials Engineering *10***(1): 10. DOI: 10.1186/s40712-015-0037-8.

[33] A. AMBROZIAK and M. KORZENIOWSKI, (2010) *"Using Resistance Spot Welding for Joining Aluminium Elements in Automotive Industry"* **Archives of Civil and Mechanical Engineering *10***(1): 5–13. DOI: 10.1016/S1644-9665(12)60126-5.

[34] American Welding Society. *Welding Handbook*. en. London: Macmillan Education UK, 1976. DOI: 10.1007/978-1-349-03073-6.

[35] H. Gaul, G. Weber, and M. Rethmeier, (2011) *"Influence of HAZ cracks on fatigue resistance of resistance spot welded joints made of advanced high strength steels"* **Science and Technology of Welding and Joining *16***(5): 440–445. DOI: 10.1179/1362171810Y.0000000031.

[36] L. Chen, Y. Zhang, X. Xue, B. Wang, J. Yang, Z. Zhang, N. Tyrer, and G. C. Barber, (2022) *"Investigation on shearing strength of resistance spot-welded joints of dissimilar steel plates with varying welding current and time"* **Journal of Materials Research and Technology *16***: 1021–1028. DOI: 10.1016/j.jmrt.2021.12.079.

[37] T. R. Mahmood, Q. M. Doos, and A. Al-Mukhtar, (2018) *"Failure Mechanisms and Modeling of Spot Welded Joints in Low Carbon Mild Sheets Steel and High Strength Low Alloy Steel"* **Procedia Structural Integrity *9***: 71–85. DOI: 10.1016/j.prostr.2018.06.013.

[38] K. M. Daws, M. H. Al-Saadi, and I. K. A. Al-Naimi, (2023) *"Investigation Parameters of Resistance Spot Welding For AA1050 Aluminum Alloy Sheets"* **Journal of Engineering *18***(10): 1128–1141. DOI: 10.31026/j.eng.2012.10.04.

[39] E. A. Fenton. "Recommended practices for resistance welding". In: 1966.

[40] U. Eşme, (2009) *"Application of Taguchi Method for the Optimization of Resistance Spot Welding Process"* **Arabian Journal for Science & Engineering (Springer Science & Business Media BV) *34***:

[41] S. M. Manladan, F. Yusof, S. Ramesh, M. Fadzil, Z. Luo, and S. Ao, (2017) *"A review on resistance spot welding of aluminum alloys"* **International Journal of Advanced Manufacturing Technology *90***(1-4): 605–634. DOI: 10.1007/s00170-016-9225-9.

[42] S. K. Hussein and O. S. Barrak, (2015) *"Analysis and optimization of resistance spot welding parameter of dissimilar metals mild steel and aluminum using design of experiment method"* **Engineering and Technology Journal** *33*(8): 1999–2011.

[43] Y. Qin, S. Xiao, L. Lu, B. Yang, X. Li, and G. Yang, (2020) *"Structural Stress–Fatigue Life Curve Improvement of Spot Welding Based on Quasi-Newton Method"* **Chinese Journal of Mechanical Engineering** *33*(1): 36. DOI: 10.1186/s10033-020-00453-3.

[44] S. Kalmykova. "SIMULATION OF T-JOINTS BETWEEN RHS STEEL MEMBERS WITH OFFSET IN ABAQUS CAE". In: 2021.

[45] H. Abdulsalam, (2021) *"Mesh Sensitivity Assessment on 2D and 3D Elastic Finite Element Analysis on a Compact Tension Specimen Geometry Using Abaqus/CAE Software"* **IOP Conference Series: Earth and Environmental Science** *730*(1): 012032. DOI: 10.1088/1755-1315/730/1/012032.

[46] R. Beckmann, R. Mella, and M. Wenman, (2013) *"Mesh and timestep sensitivity of fracture from thermal strains using peridynamics implemented in Abaqus"* **Computer Methods in Applied Mechanics and Engineering** *263*: 71–80. DOI: 10.1016/j.cma.2013.05.001.

[47] ASM Handbook Committee. *Fatigue and Fracture*. en. ASM International, 1996. DOI: 10.31399/asm.hb.v19.9781627081931.

[48] S. Mirsalehi and a. Kokabi, (2010) *"Fatigue life estimation of spot welds using a crack propagation-based method with consideration of residual stresses effect"* **Materials Science and Engineering: A** *527*(23): 6359–6363. DOI: 10.1016/j.msea.2010.06.070.

[49] A. M. Al-Mukhtar, (2016) *"Mixed-Mode Crack Propagation in Cruciform Joint using Franc2D"* **Journal of Failure Analysis and Prevention**: 1–7. DOI: 10.1007/s11668-016-0094-1.

[50] F. Badkoobeh, A. Nouri, H. Hassannejad, and H. Mostaan, (2020) *"Microstructure and mechanical properties of resistance spot welded dual-phase steels with various silicon contents"* **Materials Science and Engineering: A** *790*: 139703. DOI: 10.1016/j.msea.2020.139703.

[51] X.-C. Liu, G.-P. Chen, L. Xu, C. Yu, and Z.-q. Jiang, (2021) *"Seismic performance of blind-bolted joints for square steel tube columns under bending-shear"* **Journal of Constructional Steel Research** *176*: 106395. DOI: 10.1016/j.jcsr.2020.106395.

[52] H. Long, Y. Hu, and X. Jin, (2018) *"Stress intensity factor solutions and fatigue estimation for dual phase and low-carbon steel spot weld"* **Theoretical and Applied Fracture Mechanics**:

[53] J. Xu, Y. S. Zhang, L. Xinmin, and G. L. Chen, (2008) *"Experimental investigation of fatigue performance of spot welded dual phase sheet steels"* **Science and Technology of Welding and Joining** *13*(8): 726–731. DOI: 10.1179/174329307X236841.

[54] S. Daneshpour, S. Riekehr, M. Koçak, and C. H. J. Gerritsen, (2009) *"Mechanical and fatigue behaviour of laser and resistance spot welds in advanced high strength steels"* **Science and Technology of Welding and Joining** *14*(1): 20–25. DOI: 10.1179/136217108X336298.

[55] M. Vural, A. Akkuş, and B. Eryürek, (2006) *"Effect of welding nugget diameter on the fatigue strength of the resistance spot welded joints of different steel sheets"* **Journal of Materials Processing Technology** *176*(1-3): 127–132. DOI: 10.1016/j.jmatprotec.2006.02.026.

[56] M. H. Sar, M. H. Ridha, I. M. Husain, O. S. Barrak, and S. K. Hussein, (2022) *"Influence of Welding Parameters of Resistance Spot Welding on Joining Aluminum with Copper"* **International Journal of Applied Mechanics and Engineering** *27*(2): 217–225. DOI: 10.2478/ijame-2022-0029.

[57] I. K. Al Naimi, M. H. Al Saadi, K. M. Daws, and N. Bay, (2015) *"Influence of surface pretreatment in resistance spot welding of aluminum AA1050"* **Production & Manufacturing Research** *3*(1): 185–200. DOI: 10.1080/21693277.2015.1030795.

[58] I. M. Husain, M. L. Saad, O. S. Barrak, S. K. Hussain, and M. M. Hamzah, (2021) *"Shear force analysis of Resistance Spot Welding of Similar and Dissimilar Material: copper and carbon steel"* **IOP Conference Series: Materials Science and Engineering** *1105*(1): 012055. DOI: 10.1088/1757-899X/1105/1/012055.